Available online at www.sciencedirect.com
SCIENCE DIRECT®
Journal of Molecular Catalysis A: Chemical 223 (2004) 185–194
JOURNAL OF MOLECULAR CATALYSIS A: CHEMICAL
www.elsevier.com/locate/molcata

Noble metals intercalated/supported mica catalyst – synthesis and characterization

Thiripuranthagan Sivakumar[a,*], Thangavelu Krithiga[b], Kannan Shanthi[b], Tohru Mori[c], Jun Kubo[c], Yutaka Morikawa[c]

[a] *Department of Chemical Engineering, Anna University, Chennai 600 025, Tamil Nadu, India*
[b] *Department of Chemistry, Anna University, Chennai 600 025, Tamil Nadu, India*
[c] *Chemical Resources Laboratory, Tokyo Institute of Technology, Nagatsuta, Yokohama 226-8503, Tokyo, Japan*

Received 4 March 2003; received in revised form 27 October 2003; accepted 2 November 2003
Available online 11 September 2004

Abstract

Sodium fluorotetrasilicic mica $Na[Mg_{2.5}Si_4O_{10}F_2]$, is a 2:1 type synthetic swelling layer lattice silicate. Noble metals such as Pd and Pt–Sn were reduced in situ in surfactant exchanged fluorotetrasilicic mica (TSM). Pt and Pd were also impregnated over different supports. Both the intercalated and impregnated catalysts using noble metals such as Pd, Pt, etc. were prepared and characterized by XRD, BET surface area and TEM analysis. XRD and TEM analyses confirmed the formation of nanoparticles and the particle size was determined by the TEM measurements.

Keywords: Nanoparticles; Fluorotetrasilicic mica; Surfactant; Intercalation.

1. Introduction

Transition metals and noble metals immobilized/intercalated in the interlamellar spaces of clay minerals (mica) are expected to have the same shape selectivity as metal immobilized zeolites. In these metal immobilized zeolites, shape selectivity is exploited by the porous structure of such materials [1,2]. If the intercalated noble metals are of nanosize (1–50 nm), the catalytic activity of these catalysts will be improved due to the quantum size effect. Thus the nanostructured noble metal nanoparticles generated in the interlamellar space of the layer lattice silicates are of great interest from both fundamental and practical viewpoints. They catalyze many reactions and allow not only liquid phase but also the gas phase catalytic reactions. Since the interlayer regions are identified as reaction centre for the next generation catalysts, numbers of intercalated/immobilized catalysts have been developed in recent years [3].

Nanoparticles hold promise for use as advanced materials with new electronic, magnetic, optic and thermal properties [4,5]. Their catalytic activity and selectivity are strongly affected by their particle size [6,7]. Due to their large surface area, nanoparticles of precious metals have high catalytic activity. By systematically varying particle size, it is possible to obtain the catalyst with the required activity. Thus to determine the physical and chemical properties of these nanoparticles, especially the size dependent properties, precise control of the particle size is required [8,9]. Appropriate choice of the kind and the concentration of the reducing agent are important in controlling the particle size as increase in concentration of the reducing agent increases the reduction rate of metal ions thus leads to smaller metal nanoparticles [10]. Since the particle size of active metals improves the catalytic properties, there is much focus on the development of such new catalytic materials.

The usual synthetic technique for making such nanoparticles involves chemical or electrochemical reduction of metal ions in the presence of stabilizers such as linear polymers, ligands, surfactants, tetraalkyl ammonium salts

* Corresponding author. Tel.: +91 44 22203529.
E-mail address: sivakumar@annauniv.edu (T. Sivakumar).

1381-1169/$ – see front matter © 2004 Elsevier B.V. All rights reserved.
doi:10.1016/j.molcata.2003.11.041

or heterogeneous supports which prevent the nanoparticles from aggregating, as the aggregation of the particles leads to the reduction in their catalytic activity.

Due to the interlamellar swelling property and the adsorption capacity of clay minerals, size-quantized nanoparticles of catalytically active noble metals may be generated in the interlamellar space. Thus the noble metal containing clay minerals play a significant role in the studies of the heterogeneous catalytic reactions. Recently the need of new catalytic materials has received special interest in the layer lattice silicates because of their ion exchange properties and their expandable layer structures.

Dekany et al. have generated the nanoparticles of Pd in Montmorillonites by intercalating the noble metal precursors in the interlamellar space and reducing it by ethanol [11]. The same group generated such nanoparticles of noble metals, semi conductors and transition metals in number of layered silicate materials and characterized thoroughly by various physicochemical techniques and recently tested for their catalytic activities for selective hydrogenation of crotonaldehyde and cinnamaldehyde [12–17].

Sodium-type of fluorotetrasilicic mica (Na-TSM), $Na[Mg_{2.5}Si_4O_{10}F_2]$, a 2:1 synthetic swelling layer lattice silicate material contains two tetrahedral silicate layers and one octahedral metal oxide layer. The silicate sheets are negatively charged which are compensated by the cations (mostly Na^+ or Ca^{2+}) incorporated in the interlamellar spaces. They are easily exchangeable with any desired cations due to its cation exchange property. Lack of acid sites on the silicate sheets and swelling character in water lend itself as a good host material for the exchange/intercalation of noble metals and transition metals in its interlamellar space. The structure of sodium TSM is given in Fig. 1. It was synthesized by Kitajima and Daimon [18] and was crystallographically established by Toraya et al. [19].

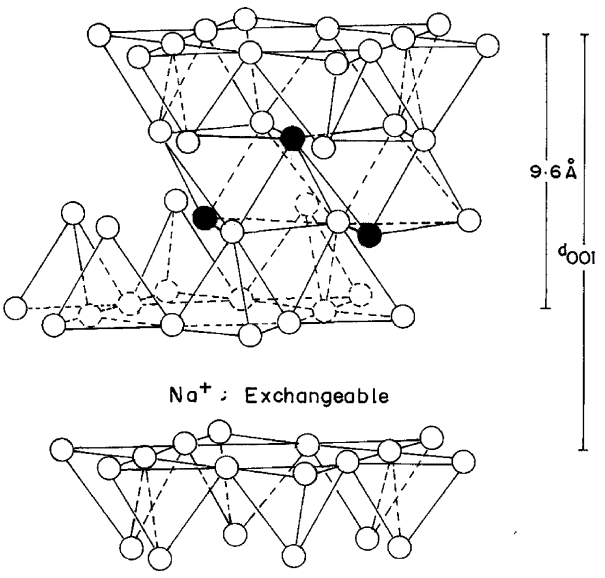

Fig. 1. Structure of fluorotetrasilicic mica.

Number of catalytic reactions have also been carried out by Morikawa et al. by exchanging Na^+ ions in TSM for number of transition metals [20–25].

In the present study, we exchanged Na-TSM with a surfactant (hexadecylpyridinium chloride) and intercalated the noble metal precursors and then reduced in situ to zerovalent metal either by alcohol or by sodium borohydride. Since Na-TSM also behaves as a very good support material, the transition metals and noble metals like Pd and Pt have also been impregnated in different amounts over Na-TSM and were characterized by various physico-chemical techniques such as XRD, XRF, TEM, BET surface area and acidity studies.

2. Experimental

2.1. Catalyst preparation

Sodium-type fluorotetrasilicic mica (Na-TSM), $Na[Mg_{2.5}Si_4O_{10}F_2]$ supplied by Topy Industry Co. Ltd. (Japan) was further purified by dispersion-sedimentation method to remove crystobalite and other non-swelling materials. The easily exchangeable interlayer Na^+ ions were exchanged by stirring Na-TSM with slightly larger amount of 1-hexadecylpyridinium bromide (HDP) (Kanto chemical) for 14 h. After the completion of exchange of Na^+ ions for HDP in the interlamellar space, the white precipitate (HDP–TSM) obtained was washed repeatedly with water and dried at 423 K. A requisite amount of HDP–TSM was taken in toluene and refluxed for 1 h in inert atmosphere (flow rate of nitrogen = 65 ml/min) [26]. The scheme of synthesis of Pd nanoparticles in Na-TSM is given in Fig. 2.

To prepare different intercalated levels of Pd in the interlamellar space of HDP–TSM, different amounts of palladium acetate in toluene were added and the mixture was refluxed for another 1 h. Ethanol served as a reducing agent for Pd ions. The black suspension containing the nanoparticles of Pd metal was washed several times with toluene, filtered and dried at 423 K. H_2PtCl_6 was used as a precursor for intercalating Pt into HDP–TSM. Different amounts of aqueous solution of $SnCl_2{\cdot}2H_2O$ were also added to incorporate Sn into the interlamellar space. Then aqueous solution of sodium borohydride was used as a reducing agent. The supported catalysts such as Pd/SiO_2, Pt/SiO_2 and Pd/Na-TSM were also prepared by ion exchange with ammonical solution of $[Pd(NH_3)_4]Cl_2$ or $[Pt(NH_3)_4]Cl_2$, respectively. The solids obtained after 24 h of thorough stirring were filtered and dried in air oven overnight at 383 K.

2.2. Catalyst characterization

2.2.1. XRD measurements

The catalysts before and after intercalation were X-ray diffracted using Rigaku RAD-IB powder diffractometer using Cu Kα radiation with λ = 0.15406 nm operated at 35 kV

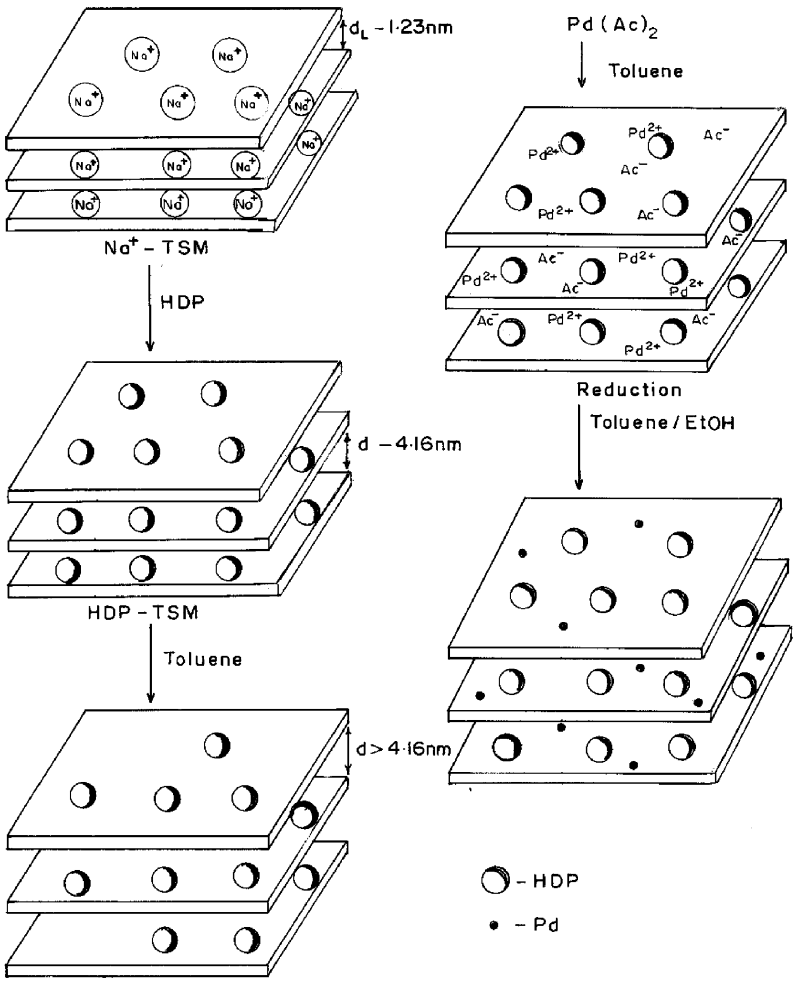

Fig. 2. Schematic illustration of synthesis of Pd-nanoparticles in Na-TSM.

and 25 mA in 2θ range of 0.9–60° at the scanning rate of 1°/min. The basal distances d_L were computed from Bragg reflection (0 0 1) and palladium and platinum particles show (1 1 1) peak at 40°.

2.2.2. XRF analysis

The content of noble metals in the catalysts was determined by X-ray fluorescence analyzer (Shimadzu EDX-800). Catalyst samples (50 mg) were pelletted using a die and taken in the cell of XRF instrument for further determination.

2.2.3. Transmission electron microscopic measurements

Transmission electron micrographs were taken to find out the particle size of the metal particles. JEOL JEM-2010F field emission microscope with an operating voltage of 200 kV was used in the experiment. One drop of very dilute propanol was used to make the suspension of the catalyst and the samples was placed on the copper grid and allowed to dry. After the alcohol evaporation, electron micrographs were taken for the particles on the grid. The average particle size was calculated by taking 100–150 particles on TEM images.

2.2.4. BET surface area analysis

The intercalated and impregnated catalysts were pretreated with nitrogen at 448 and 873 K, respectively for 2 h and cooled down to room temperature and a mixture of nitrogen and helium (30:70) was used as an adsorbate to find out the BET surface area. Micromeritics (2700) BET surface area analyzer fitted with thermal conductivity detector was used in the experiment.

2.2.5. Temperature-programmed desorption measurements

The acidity of the samples was determined using ammonia as probing molecule. The samples were first out-gassed for 2 h at 200 °C temperature at 10^{-7} Torr pressure. The temperature of the samples was brought down to room temperature and ammonia was then admitted into the cell until complete saturation. The samples were again degassed at 60 °C under vacuum to remove the physisorbed ammonia. Small amount of adsorbed sample was taken in an empty tube connected to the GC column fitted with TCD detector. The temperature of the sample was slowly increased from room temperature to

Table 1
Structural properties of various Pd and Pt catalysts

Catalyst	Pd or Pt content (wt.%)	BET surface area (m^2/g)	Particle size of Pd (nm)
Na-TSM	–	5.5	–
HDP–TSM	–	4.0	–
Pd/Na-TSM	1.5	5.0	–
Pd–HDP–TSM(1)	0.5	4.1	3.5[a]
Pd–HDP–TSM(2)	1.0	4.0	4.2[a]
Pd–HDP–TSM(3)	2.2	3.8	7.8[a]
Pd/SiO_2	1.0	230 (310)	6.6
Pt/SiO_2	1.0	226 (310)	–
Pt–HDP–TSM	0.8	3.0	–

The values in the brackets are the surface areas of the corresponding supports.
[a] Particle size calculated from TEM images obtained by TEM.

400 °C. Ammonia desorbed at different temperatures was estimated from the chromatograms. From the width and area of the peaks, acidity was calculated and total acidity is reported in Table 4.

3. Results and discussion

The BET surface area and XRF data of various catalysts are given in Tables 1–3.

3.1. X-ray diffraction measurements

Sodium tetrafluorosilicic mica being a swelling silicate material allows the easy diffusion of HDP ions for exchange. An increase in the interlamellar space is expected by the exchange of Na^+ ions by HDP, which forms HDP–TSM. Fig. 3 shows the XRD patterns of HDP–TSM which indicates a considerable increase in the basal spacing from 1.23 to 4.16 nm. These values include the thickness of the silicate layer, which is ca. 1.0 nm. However, they absorb water molecule from atmosphere and also show slightly increased basal spacing indicating the importance of drying temperature for basal spacing values. The diffraction peak corresponding to $d(0\,0\,1)$ reflection observed at 2θ around 7.0° for Na-TSM was shifted to $2\theta = 2.1°$ after the exchange of HDP. The $d(0\,0\,1)$ reflection at $2\theta = 2.1°$ for HDP–TSM increased slightly after the intercalation of the noble metals (Fig. 3). When the pretreatment temperature was increased to 573 K, a shift in $d(0\,0\,1)$ was observed. This may be due to the decomposition of HDP (Fig. 4). Fig. 5 shows the $d(1\,1\,1)$ reflections of Pd at $2\theta = 40°$ for different samples of HDP–TSM with varying percentage of Pd (0.5% Pd–HDP–TSM, 1% Pd–HDP–TSM and 2.2% Pd–HDP–TSM). The diffraction peak corresponding to $d(1\,1\,1)$ around $2\theta = 40°$ can be used for finding out the diameter of noble metal. Since HDP–TSM also show up a peak around $2\theta = 39°$, the Bragg reflection $d(1\,1\,1)$ for Pd was seen clearly only when the intercalation level exceeded 2%. Fig. 6 shows the XRD patterns of Pd–HDP–TSM pretreated at different temperatures. As the pretreatment temperature was raised from 448 to 573 K, an increase in the intensity of the peak at $2\theta = 40°$ was observed. Pd–HDP–TSM catalyst

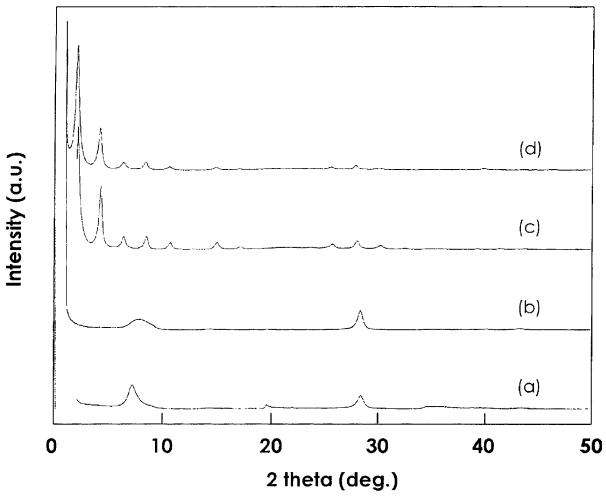

Fig. 3. XRD patterns of (a) TSM; (b) 2.1% Pd/Na-TSM; (c) HDP–TSM; (d) 2.2% Pd–HDP–TSM.

Table 2
XRF data of various Pd catalysts

Catalyst	Pd	SiO_2	$Mg_5F_4O_3$	C	Br	Na_2O
Pd/Na-TSM	1.5	59.5	33.3	0.0	0.0	5.6
Pd/Na-TSM	2.1	59.7	32.7	0.0	0.0	5.5
Pd–HDP–TSM(1)	1.0	32.6	14.0	44.2	6.2	0.0
Pd–HDP–TSM(2)	1.0	32.8	15.5	43.5	7.2	0.0
Pd–HDP–TSM(3)	2.2	31.7	13.0	46.6	6.5	0.0

Table 3
XRF data for various Pt and Sn catalysts

Catalyst	Pt	Sn	SiO_2	$Mg_5F_4O_3$	C	Br
Pt–HDP–TSM(1)	0.8	0.0	48.4	18.8	32.0	0.04
Pt–HDP–TSM(2)	5.5	0.0	40.9	21.4	32.0	0.2
Pt/Sn–HDP–TSM(1)	1.9	2.7	40.9	22.3	32.0	0.1
Pt/Sn–HDP–TSM(2)	3.4	2.2	40.0	22.2	32.0	0.2
Pt/Sn–HDP–TSM(3)	2.6	0.7	43.6	21.0	32.0	0.05

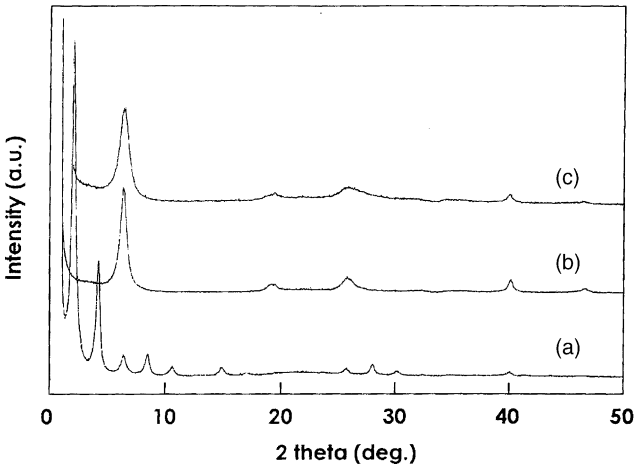

Fig. 4. XRD patterns showing the shift of $d(0\,0\,1)$ reflections of 2.2% Pd–HDP–TSM at different temperatures: (a) pretreated with hydrogen at 448 K; (b) at 573 K; (c) used up to 523 K.

Table 4
Comparison of BET surface area and acidity of Na-TSM with other clay catalysts and silica

Mineral	Surface area (m^2/g)	Peak temperature (°C)	Amount of ammonia desorbed	
			(mol/g)	(nmol/m^2)
Na-TSM	5.5	–	0.00	0.0
Bentonite	38.1	296	2.30	60.0
Hectorite	14.2	292	11.00	770.0
Silica gel	347	314	0.54	1.6

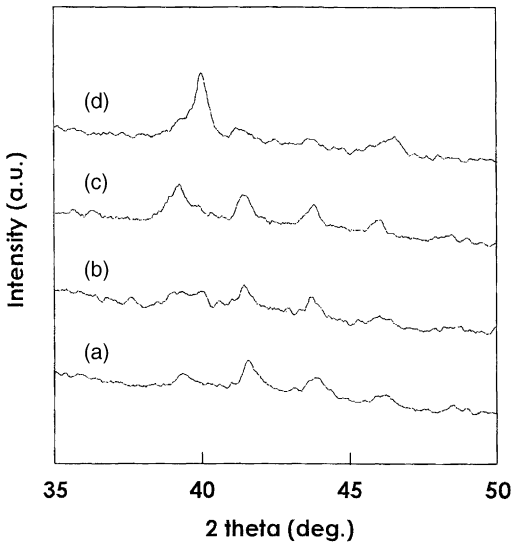

Fig. 5. XRD patterns showing $d(1\,1\,1)$ reflections of Pd at $2\theta = 40°$: (a) HDP–TSM; (b) 0.5% Pd–HDP–TSM; (c) 1% Pd–HDP–TSM; (d) 2.2% Pd–HDP–TSM.

containing 2.2 wt.% of Pd showed an intense peak at $2\theta = 40°$ when it was pretreated with hydrogen at 573 K. This may be due to the aggregation of Pd particles after the decomposition of HDP.

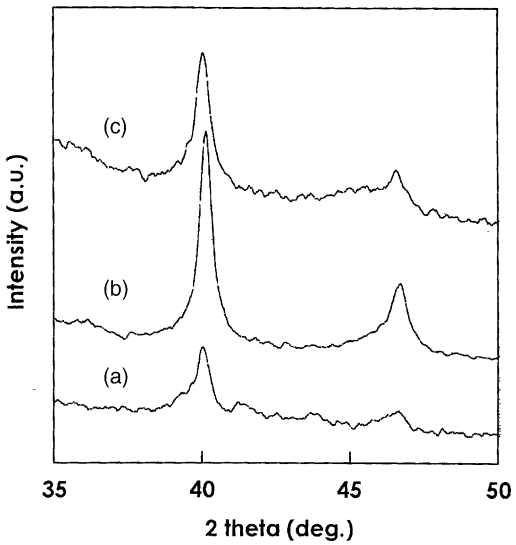

Fig. 6. XRD patterns showing the effect of pretreatment of 2.2% Pd–HDP–TSM at different temperatures on $d(1\,1\,1)$ reflection: (a) pretreated with hydrogen at 448 K; (b) at 573 K; (c) used up to 523 K.

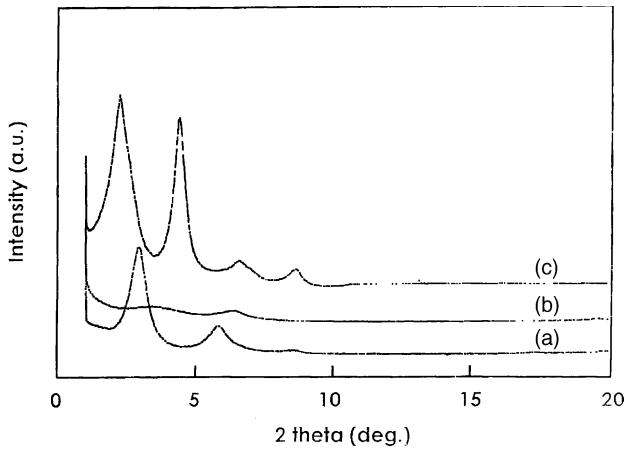

Fig. 7. XRD patterns of Pt and Sn catalysts: (a) 3.2% Sn–HDP–TSM; (b) 5.5% Pt–HDP–TSM; (c) HDP–TSM.

The XRD patterns of Pt and Sn catalysts are shown in Figs. 7 and 8. Diffraction peak corresponding to $d(0\,0\,1)$ reflection for Pt/Sn–HDP–TSM was also observed at $2\theta = 40°$ which decreased as the percentage of Sn increased.

3.2. Transmission electron microscopic measurements

The formation of nanoparticles can be confirmed by the transmission electron micrographs. The TEM photograph of Pd–HDP–TSM shows that the Pd particles are well

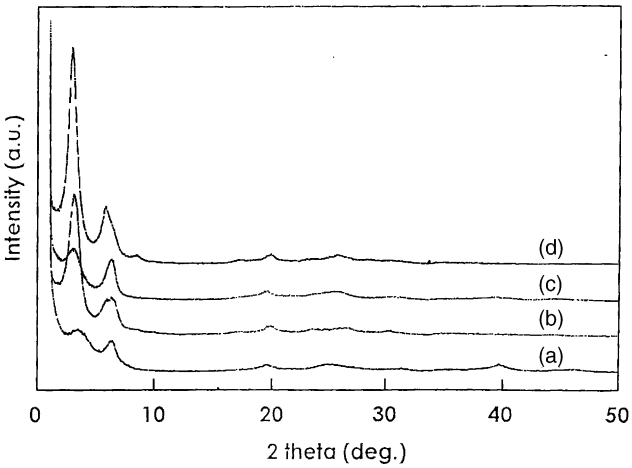

Fig. 8. XRD patterns of Pt and Sn catalysts: (a) 5.5% Pt–HDP–TSM; (b) Pt/Sn (1.5)–HDP–TSM; (c) Pt/Sn (3.7)–HDP–TSM; (d) Pt/Sn (0.6)–HDP–TSM.

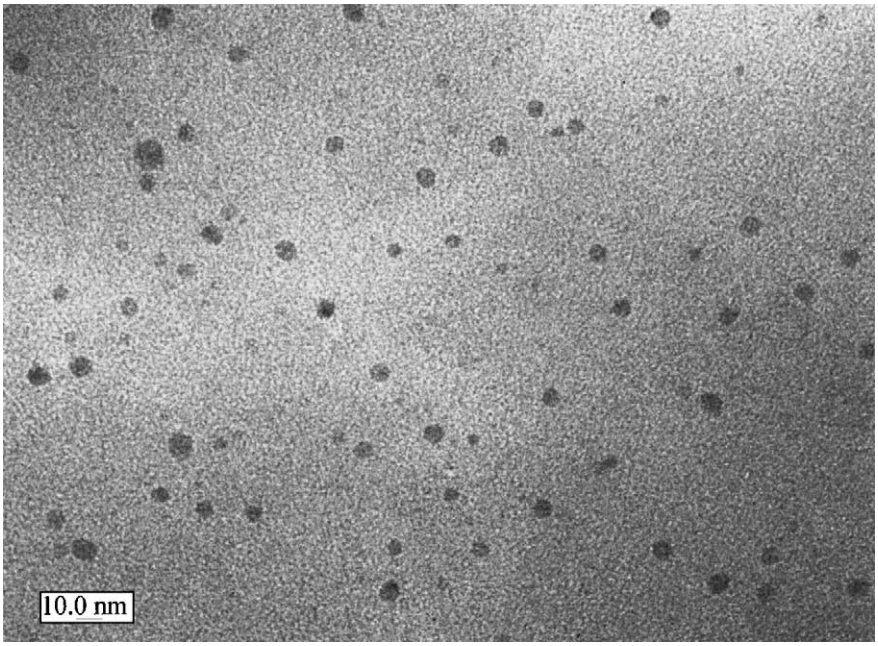

Fig. 9. TEM image of 0.5% Pd–HDP–TSM.

monodispersed and they are of nanosized (Fig. 9). The particle size of Pd increased with the intercalation level of Pd (Figs. 10 and 11). Dispersion was not so good and aggregation of metal particles at different places was seen for the catalysts in which there is no HDP. Fig. 12 shows TEM image of 1.5% Pd impregnated over Na-TSM, the palladium particles tend to agglomerate when they are impregnated over Na-TSM.

The TEM pictures of Pt and Sn intercalated catalysts are shown in Figs. 13–15. When either Pt or Sn was intercalated as a single metal, the size of particles was bigger than when they were introduced together. Increase in Pt content did not show an increase in particle size. The TEM image of Sn–HDP–TSM shows that the particles are not discrete. Very fine particles were obtained when the loading of Sn

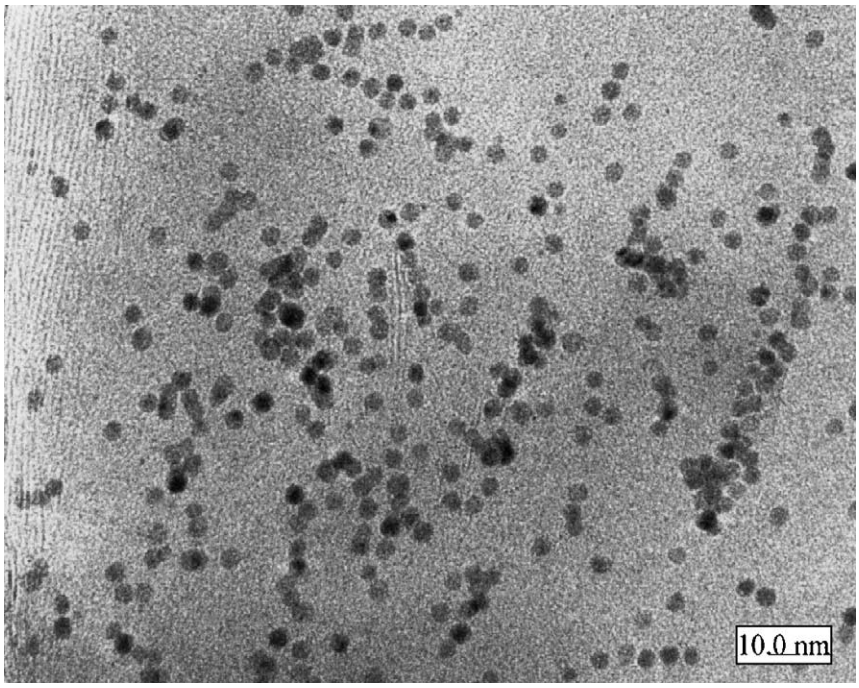

Fig. 10. TEM image of 1.0% Pd–HDP–TSM.

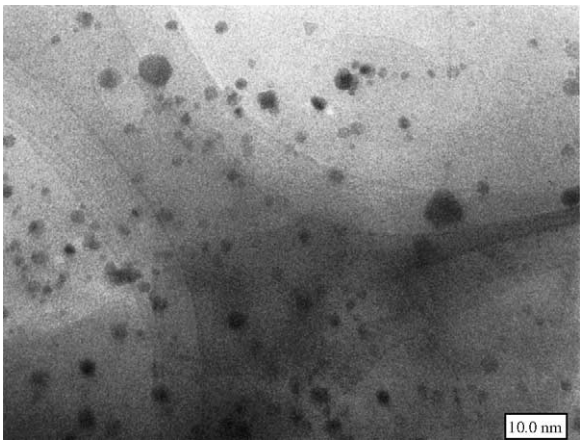

Fig. 11. TEM image of 2.2% Pd–HDP–TSM.

increases in Pt/Sn–HDP–TSM (Figs. 16–18). From this it can be inferred that catalysts can be synthesized with the particle size of the order of 1 nm by intercalating Pt and Sn together in HDP–TSM.

The TEM measurement reveals that in the metal loading of HDP–TSM catalysts, the metal particles are present on both external and internal surfaces. The particles may also be present on the external surface when the metal loading was increased. However, at lower loading of Pd, nanoparticles of metal were formed in the interlamellar space.

3.3. BET surface area measurements

BET surface area of various Pd and Pt catalysts are given in Table 1. The values given in the brackets are the surface area of corresponding supports. Pd and Pt content (wt.%)

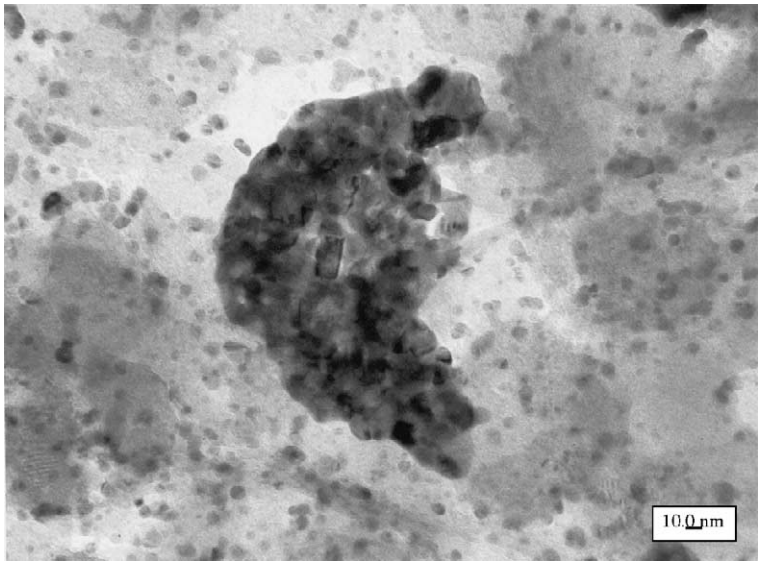

Fig. 12. TEM image of 1.5% Pd/Na-TSM.

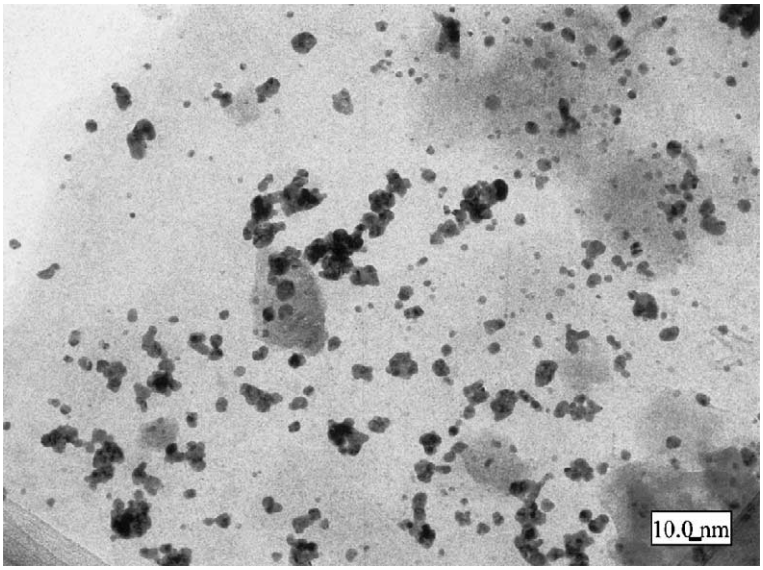

Fig. 13. TEM image of 0.8% Pt–HDP–TSM.

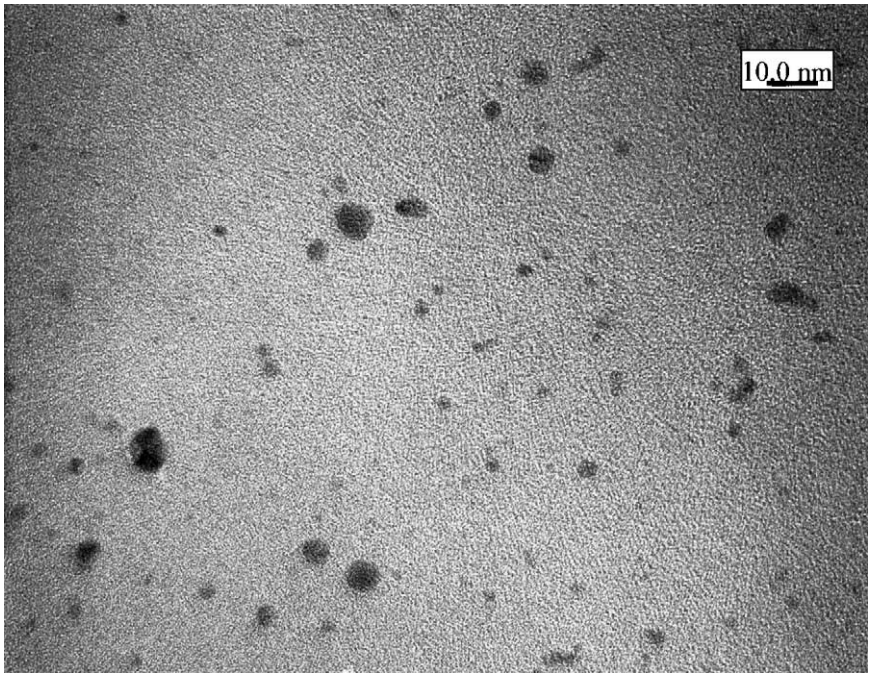

Fig. 14. TEM image of 5.5% Pt–HDP–TSM.

determined by XRF and the particles size measured by TEM studies for various catalysts are also given in the table. This table clearly indicates that all the TSM catalysts show very low BET surface area values. Impregnation or intercalation of noble metals does not affect the surface area of TSM catalysts. However when the support was SiO_2 the impregnation of either Pt or Pd decreased the surface area. It can also be seen from the table that the average particle size of Pd increased slightly when the intercalation level of Pd increased in HDP–TSM.

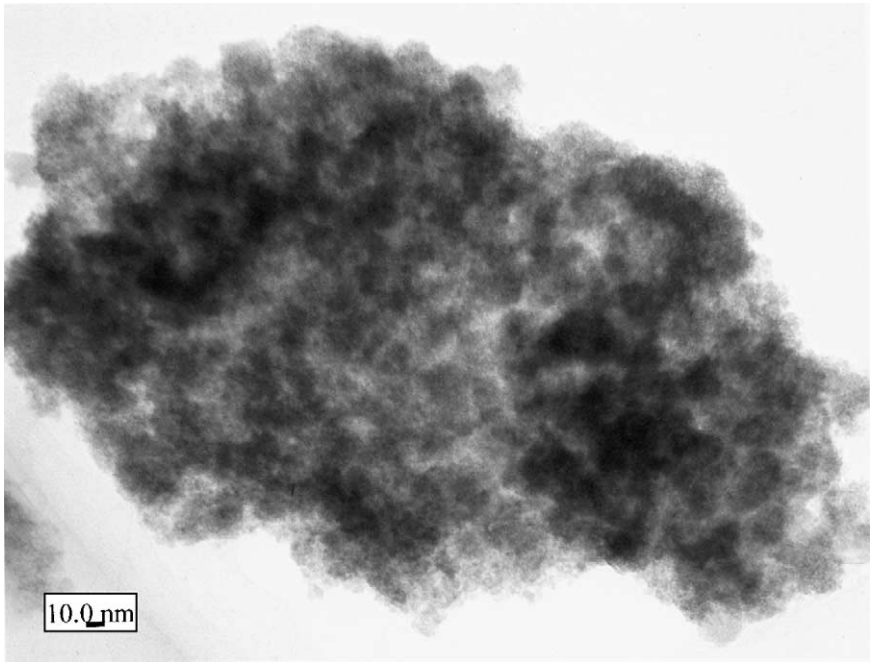

Fig. 15. TEM image of 3.2% Sn–HDP–TSM.

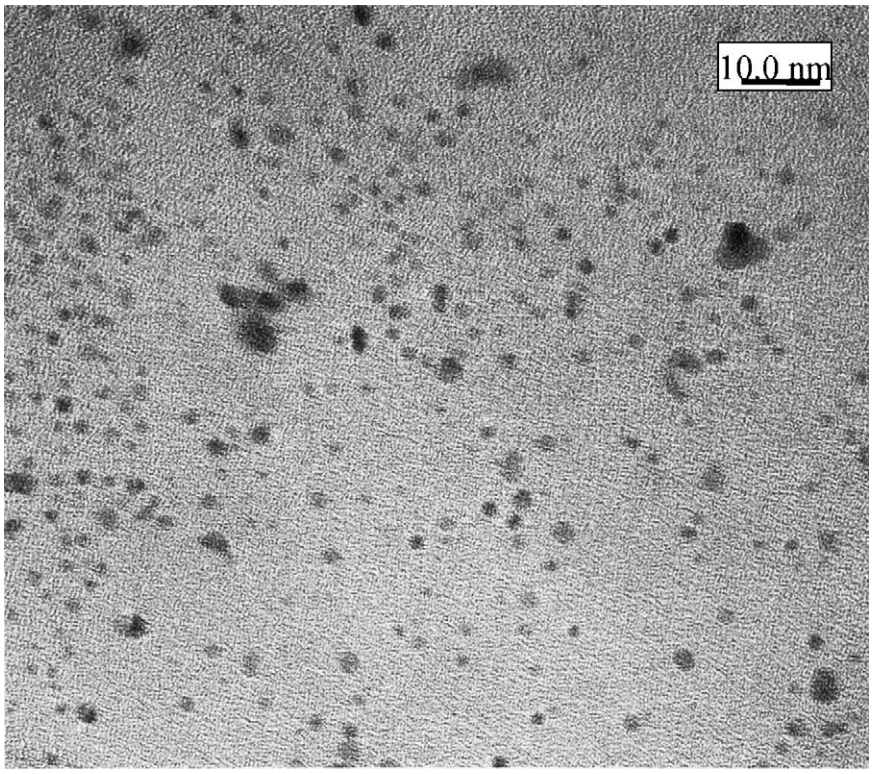

Fig. 16. TEM image of Pt/Sn (3.7)–HDP–TSM.

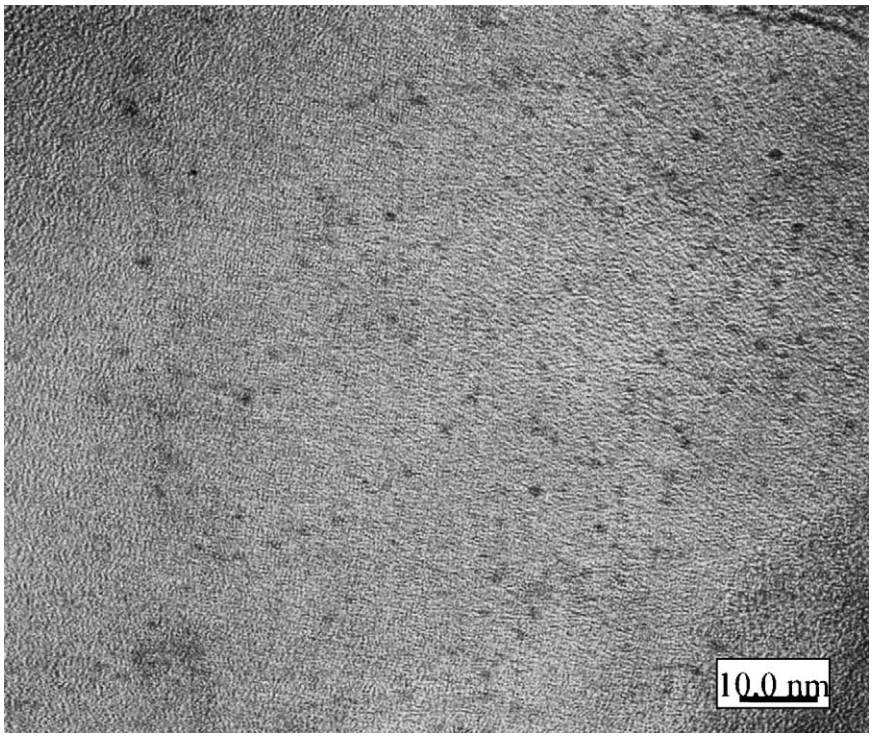

Fig. 17. TEM image of Pt/Sn (1.5)–HDP–TSM.

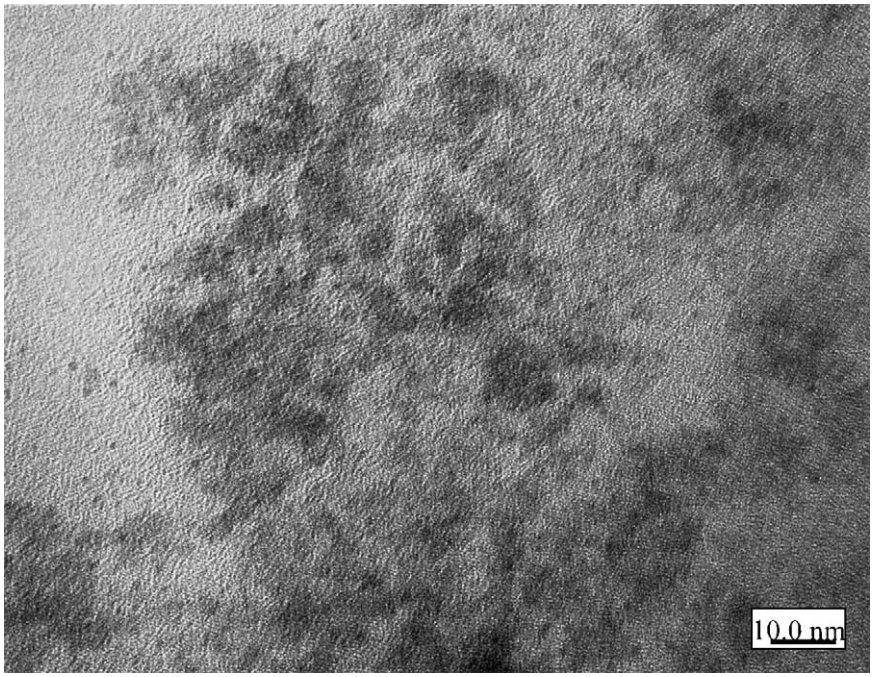

Fig. 18. TEM image of Pt/Sn (0.6)–HDP–TSM.

3.4. Temperature-programmed desorption measurements

Among the various clay catalysts tested all the catalysts show acidity except TSM, this confirms that silicate sheets of TSM are non acidic. Catalytic tests using the intercalated catalysts are underway.

4. Conclusion

Different levels of Pd have been intercalated into interlamellar spaces of the silicate sheets and also the nanoparticles could be obtained by the in situ reduction using ethanol as reducing agent. TEM photographs confirm the synthesis of nanosized particles in the interlamellar space.

XRD patterns reveal that exchange of HDP ions into the interlamellar space increase the basal spacing. The pretreatment temperature of Pd–HDP–TSM was limited up to 473 K because decomposition of HDP takes place above 473 K. Acidity studies reveals that there is lack of acid sites in the silicate sheets of TSM. As far as Pt/Sn–HDP–TSM catalysts are concerned, very fine and discrete particles were obtained when they were introduced together.

References

[1] P. Gallezot, A. Giroir-Fendler, D. Richard, Catal. Lett. 5 (1990) 169.
[2] D.G. Blackmond, R. Oukaci, B. Blanc, P. Gallezot, J. Catal. 131 (1991) 401.
[3] T. Sivakumar, T. Mori, J. Kubo, Y. Morikawa, Chem. Lett. (2001) 860.
[4] V.L. Colvin, M.C. Schlamp, A.P. Alivisatos, Nature 370 (1994) 354.
[5] R.P. Andres, Chem. Eng. News (1992) 18.
[6] Y.M. Tricokot, J.H. Fendler, J. Am. Chem. Soc. 106 (1984) 7359.
[7] M. Meyer, C. Wallberg, K. Kurihara, J.H. Fendler, J. Chem. Soc. Chem. Commun. (1984) 90.
[8] I. Dekany, L. Turi, E. Tombacz, J.H. Fendler, Langmuir 11 (1995) 2285.
[9] I. Dekany, L. Nagy, L. Turi, Z. Kiraly, N.A. Kotov, J.H. Fendler, Langmuir 12 (1996) 3709.
[10] T. Teranishi, M. Mujake, Chem. Mater. 10 (1998) 594.
[11] I. Dekany, L. Turi, Z. Kiraly, Appl. Clay Sci. 15 (1999) 221.
[12] G. Szollosi, I. Kun, A. Mastalir, M. Bartok, I. Dekany, Solid State Ionics 142 (2001) 273.
[13] A. Szucs, F. Berger, I. Dekany, Coll. Surf. A 174 (2000) 387.
[14] A. Mastalir, Z. Kiraly, G. Szollosi, M. Bartok, Appl. Catal. A 213 (2001) 133.
[15] S. Papp, A. Szucs, I. Dekany, Solid State Ionics 142 (2001) 169.
[16] I. Dekany, L. Turi, A. Szucs, Z. Kiraly, Coll. Surf. A 141 (1998) 405.
[17] S. Papp, A. Szucs, I. Dekany, Appl. Clay Sci. 19 (2001) 155.
[18] K. Kitajima, M. Daimon, Nippon Kagaku Kaishi (1975) 991.
[19] H. Toraya, S. Iwai, F. Marumo, M. Daimon, R. Kondo, Kristallogr. Kristallgeom. Kristallphys. Kristallchem. 44 (1976) 42.
[20] Y. Morikawa, T. Goto, Y. Moro-oka, T. Ikawa, Chem. Lett. (1982) 1667.
[21] Y. Morikawa, K. Takagi, Y. Moro-oka, T. Ikawa, Chem. Lett. (1982) 1805.
[22] K. Takagi, Y. Morikawa, T. Ikawa, Chem. Lett. (1985) 527.
[23] F. Wang, W. Ueda, Y. Morikawa, T. Ikawa, Chem. Lett. (1990) 405.
[24] Y. Morikawa, A. Yasuda, Y. Moro-oka, T. Ikawa, Chem. Lett. (1983) 1911.
[25] Y. Morikawa, Adv. Catal. 39 (1993) 303.
[26] Z. Kiraly, I. Dekany, A. Mastalir, M. Bartok, J. Catal. 161 (1996) 401.